Electronic Supplementary Material (ESI) for Chemical Science.

Supplementary Information

A Highly Contorted Push-Pull Naphthalenediimide Dimer and Evidence of Intramolecular Singlet Exciton Fission

Deepak Bansal[1†], *Arup Kundu*[2†], *Vijay Pal Singh*[1], *Arun K. Pal*[3], *Ayan Datta*[3*], *Jyotishman Dasgupta*[2*], *Pritam Mukhopadhyay*[1*]

[1]Supramolecular and Material Chemistry Lab, School of Physical Sciences, Jawaharlal Nehru University, New Delhi 110067, India

[2]Department of Chemical Sciences, Tata Institute of Fundamental Research, Mumbai 400005, India

[3]School of Chemical Sciences, Indian Association for the Cultivation of Science, Kolkata 700032, West Bengal, India

Contents **Page No**

Materials and Methods:

General: Chemicals were sourced either from Sigma-Aldrich, or TCI chemicals, India and were used as received. The reactions for the synthesis of **PPD** were carried out in a heavy-wall Wheaton glass vials (4 ml) sourced from Sigma Aldrich. Thin layer chromatography (TLC) was carried out on aluminium plates coated with silica gel mixed with fluorescent indicator and was sourced from Merck, Germany. NMR (^{1}H, ^{13}C) spectra were recorded on a Bruker 500 MHz spectrometer in $CDCl_3$ with TMS as a standard. Spin multiplicities are reported as a singlet (s), doublet (d), and triplet (t) with coupling constants (J) given in Hz, or multiplet (m). ESI-HRMS spectral data were obtained using a Waters make ESI-MS model Synapt G2 high definition mass spectrometry. Absorption studies were performed on a JASCO V-670 UV-vis-NIR Spectrophotometer. All the spectroscopic experiments were carried out in UV Grade solvents which was sourced from Spectrochem, India. The FTIR spectra were recorded with a Perkin–Elmer FTIR 2000 or spectrum–two spectrometer. **PP-NDI** was prepared according to the earlier reported synthesis.[1]

Cyclic and Differential Pulse Voltammetry (CV/DPV): CV and DPV were carried out using a computer controlled potentiostat (CHI 650C) and a standard three electrode arrangement that consisted of both platinum working and auxiliary electrodes and saturated calomel (SCE) as reference electrode. All electrochemical measurements were carried out in Ar-purged DCM with n-Bu_4NPF_6 as the supporting electrolyte. CV studies of the molecules **PPD** and **PP-NDI** were performed in degassed DCM under Ar atmosphere and the scan rate for the measurements was typically 200-300 mV/s. DPV was carried out keeping peak amplitude 50 mV, peak width 0.01 sec, pulse period 0.05 sec and increment E at 20 mV.

X-ray Crystallography: The data for **PPD** and **PP-NDI** were collected on Bruker Kappa Apex-CCD diffractometer equipped with graphite monochromatic Mo-Kα radiation ($\lambda = 0.71073$ Å). The frames were collected at 298 K. The data was processed with XCalibur S Saint, and empirical absorption corrections were applied by using the spherical harmonic incorporated in the SCALE3 ABSPACK scaling algorithm. The structures were solved by direct methods using SIR-92 and refined by full-matrix least-squares refinement techniques on F^2 by using SHELXL-2018 in the WinGX module. All hydrogen atoms were fixed at the calculated positions were refined isotropically. CCDC: **2171334** (PP-NDI), **2171335** (PPD).

Steady State Absorption and emission Measurement. Steady state absorption measurements were performed using a commercial JASCO V-670 spectrophotometer in the 200 to 800 nm region. All steady state emission measurements were done in Flourolog-3 (Horiba Jobin Yvon Inc) spectrofluorometer with Xe lamp as excitation source and PMT detector.

Time resolved Emission Measurements: Lifetime measurement were done using Time Correlated Single Photon Counting (TCSPC) technique. Florescence photons were detected at the magic angle 54.7° to avoid anisotropy effects by a microchannel plate photomultiplier (model R2809; Hamamatsu Corp.) which was coupled to a single photon counting setup. The data was collected with Becker and Hickl SPC 130 card. Excitation was done at 540 nm photo excitation, with a picosecond laser pulse. The 540 nm was generated from a supercontinuum laser source (YSL photonics) for excitation. Only 543 ± 25 nm was chosen for excitation of sample using a bandpass filter. Part of the same beam was used as sync pulse. Pulse width and repetition rate was 1-2 ps and 80 MHz respectively. Instrument response function (FWHM = 172 ps) was measured by scattering photons using a colloidal suspension of dried nondairy coffee whitener. All TCSPC measurements were done using 200 µM solutions in DCM for both **PPD** and **PP-NDI**.

Ultrafast Transient Absorption Spectroscopy. Femtosecond transient pump-probe spectroscopy was carried out using a previously reported Ti-Sapphire setup (*J. Phys. Chem. Lett*. 2021, **12**, 1468−1474). Using a regenerative amplifier (Coherent Legend Elite), pulses of 30 fs time duration with 65 nm bandwidth amplified pulse at 1 kHz repetition rate were obtained. The amplified pulses with 4 mJ/pulse energy were obtained after seeding with 25 femtosecond 100 nm bandwidth laser pulses obtained from an oscillator (Micra-5 mode-locked Ti-Sapphire) operating at 80 MHz repetition rate. The amplified output was divided into two parts. One part was used to produce the femtosecond probe pulse by focusing it on a 2 mm thick sapphire crystal to generate a white light continuum (420-1600 nm). The other part was used to generate a tunable femtosecond pump pulse using an Optical Parametric Amplifier (Coherent OPeraASolo Ultrafast Optical Parametric Amplifier system). The pump beam power was attenuated to 40-400 nJ per pulse. The 400 nm pump beam was generated directly by the second harmonic generation of fundamental 800 nm output form the amplifier using a 0.2 mm thick BBO crystal. The probe beam was split into two parts. One part was used to provide a reference signal to the detector while the other part was sent through sample with the pump pulse. Due to the probe referencing the transient absorption signals were minimally affected by shot-to-shot laser fluctuation. For the transient absorption measurements, the pump and the probe beam were focused and spatially overlapped into the sample and the transmitted probe was taken to a fiber optics coupled multichannel spectrometer with CMOS (VIS) / InGaAs (NIR) sensor. A 2 mm quartz flow-cell was used with constant flow to avoid photo-degradation. The temporal resolution obtained in our transient absorption set up was close to 90 fs. The time delay between the pump and probe pulses were controlled by a motorized translation stage with quadrapass mirror assembly.

The nanosecond to microsecond transient absorption data were collected using a commercial pump-probe system (Ultrafast System, EOS), having ~800 ps time resolution. For the excitation pulse, the 1 kHz repetition rate femtosecond pulses obtained from the OPA was used. The white light supercontinuum probe (360 nm to 1600 nm, with spectral resolution of 1.5 nm (VIS) and 3.5 nm (NIR)) was generated by focusing a Nd:YAG laser pulse into a photonic crystal fiber. The probe pulses were electronically synchronized with the femtosecond regenerative amplifier, and the pump-probe delay time was controlled by a digital delay generator (CNT-90, Pendulum Instruments). To minimize the noise, the probe beam was referenced with respect to the signal channel similar to the femtosecond transient absorption measurements.

The decay kinetics was fitted with multi exponential kinetic model convoluted with IRF of 100 fs, with the help of IGOR Pro 5 and the singular value decomposition by Global and target analyses of the transient absorption data were carried out with the help of the Surface Xplorer 4 and Glotaran 1.5.1 software.

Synthesis:

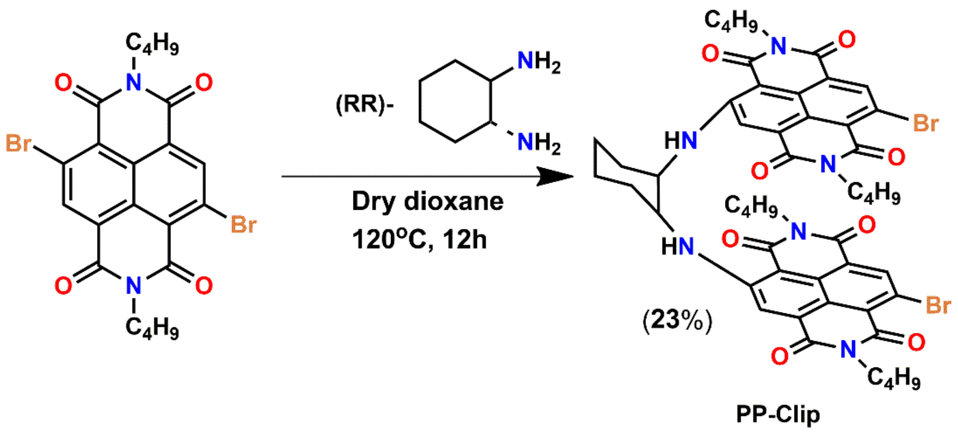

PP-Clip: A suspension of N,N-dibutyl-2,3-dibromo-naphthalene-1,4,5,8-tetracarboxylicacidbisimide (NDI-Br$_2$) (1.0g, 0.186 mmol) and 1R,2R-cyclohexyldiamine (0.017g, 0.148 mmol) was stirred in dry dioxane for 12 h at 110°C. The resulting red color solution was allowed to attain room temperature. The reaction mixture was filtered and the solvent was removed under reduced pressure to afford red solid. The solid compound was washed with methanol and air-dried followed by its purification by silica column chromatography (230-400 mesh) using CHCl$_3$/MeOH (9:1) as the eluent to obtain reddish pink colored compound. Yield = 23% (220 mg). R_f = 0.78 (8:2 CHCl$_3$/MeOH). Melting Point: > 300 °C. ^{1}H NMR (500 MHz, CDCl$_3$, 300 K): δ = 10.15 (s, 2H, -NH), 8.57 (s, 2H, ArH), 8.23 (s, 2H, ArH), 4-10-3.96 (10H, AxCH$_2$ + -NHCH), 2.34 (s, 2H, -CH$_2$), 2.04 (s, 2H, -CH$_2$), 1.814 (s, 2H, -CH$_2$), 1.65 (s, 2H, -CH$_2$), 1.54-1.256 (16H, AxCH$_2$CH$_2$), 0.98-0.923 (d, 12H, -CH$_3$). ^{13}C NMR (125 MHz, CDCl$_3$, 300 K): δ = 165.39, 160.19, 151.60, 137.89, 127.70, 126.66, 122.82, 122.67, 120.92, 120.89. 120.29, 100.24, 65.82, 58.64, 41.17, 40.05, 32.43, 31.57, 29.87, 24.60, 22.61, 20.30, 15.25, 14.07. HRMS (M+ H$^+$; m/z): calc. 1023.2286, found; 1023.1380. Anal. Calcd. for C$_{50}$H$_{52}$Br$_2$N$_6$O$_8$: C, 58.60; H, 5.11; N, 8.20. Anal. Found C, 58.47; H, 5.50; N, 8.83. FTIR spectrum (Zn-Se ATR, selected peaks, cm^{-1}): 2959, 2934, 2872, 2334, 1710, 1665 and 1630. Absorption spectrum [λ$_{max}$, nm, DCM (ε x 10^5, M^{-1}cm^{-1})]: 533 (17572), 502 (17508), 368 (20182), 349 (17091), 330 (13886).

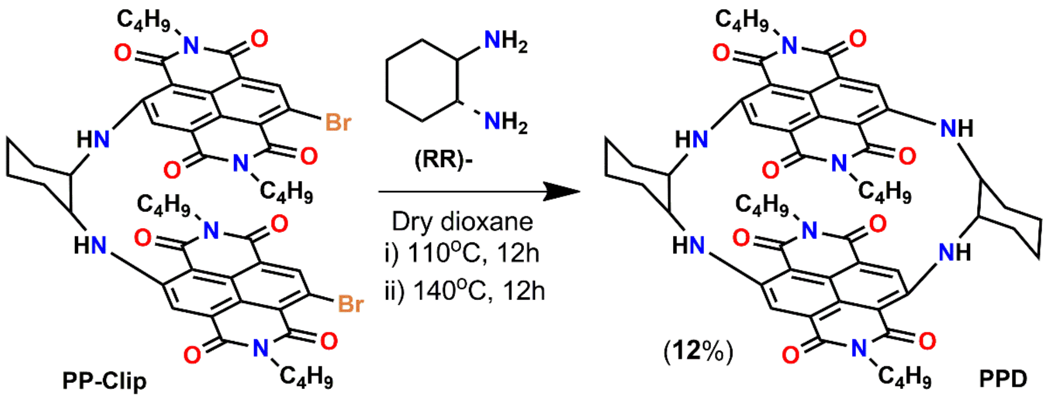

PPD: In a heavy-walled Wheaton glass vial, dry dioxane (3ml), **PP-Clip** (0.1g, 0.097 mmol) and 1R,2R-cyclohexyldiamine (0.013g, 0.117 mmol) was added and stirred for 12 h at 110°C. After 12h, the purple color reaction mixture was heated to 140°C for another 12h. The resulting blue colored solution was allowed to attain room temperature. The reaction mixture was transferred to round bottom flask using chloroform solvent and solvent was removed under reduced pressure. The purified blue coloured **PPD** was obtained by silica column chromatography (230-400 mesh) using $CHCl_3$/MeOH (9:1) as the eluent. Yield = (12 mg) 12 %. R_f = 0.78 (8:2 $CHCl_3$/MeOH). Melting Point: > 300 °C. ^{1}H NMR (500 MHz, $CDCl_3$, 300 K): δ = 9.41 (s, 4H, -NH), 7.90 (s, 4H, ArH), 4.13-4.09 (m, 4H, CyCH), 4.06-4.00 (m, 4H, AxCH$_2$), 3.90-3.86 (4H, AxCH$_2$), 2.35 (4H, CyCH$_2$), 1.99 (4H, -CyCH$_2$), 1.69 (4H, -CyCH$_2$), 1.59-1.35 (m, 20H, CH$_2$), 0.91 (m, 12H, CH$_3$). ^{13}C NMR (125 MHz, CDCl3, 300 K): δ = 165.19, 162.11, 149.20, 124.35, 119.77, 118.26, 102.84, 59.42, 40.03, 32.95, 30.08, 25.11, 20.27, 13.74. HRMS: calc. 977.1562; found (977.1568) (m/z). Anal. Calcd. for $C_{56}H_{64}N_8O_8$: C, 69.83; H, 6.60; N, 11.47. Anal. Found C, 69.45; H, 6.54; N, 11.44. FTIR spectrum (Zn-Se ATR, selected peaks, cm^{-1}): 3259 (-NH), 2954 2924, 2854, 2360, 2341, 1676, 1629. Absorption spectrum [λ_{max}, nm, DCM (ε x 10^4, $M^{-1}cm^{-1}$)]: 592 (3052), 526 (2773), 499 (2412), 366 (9708).

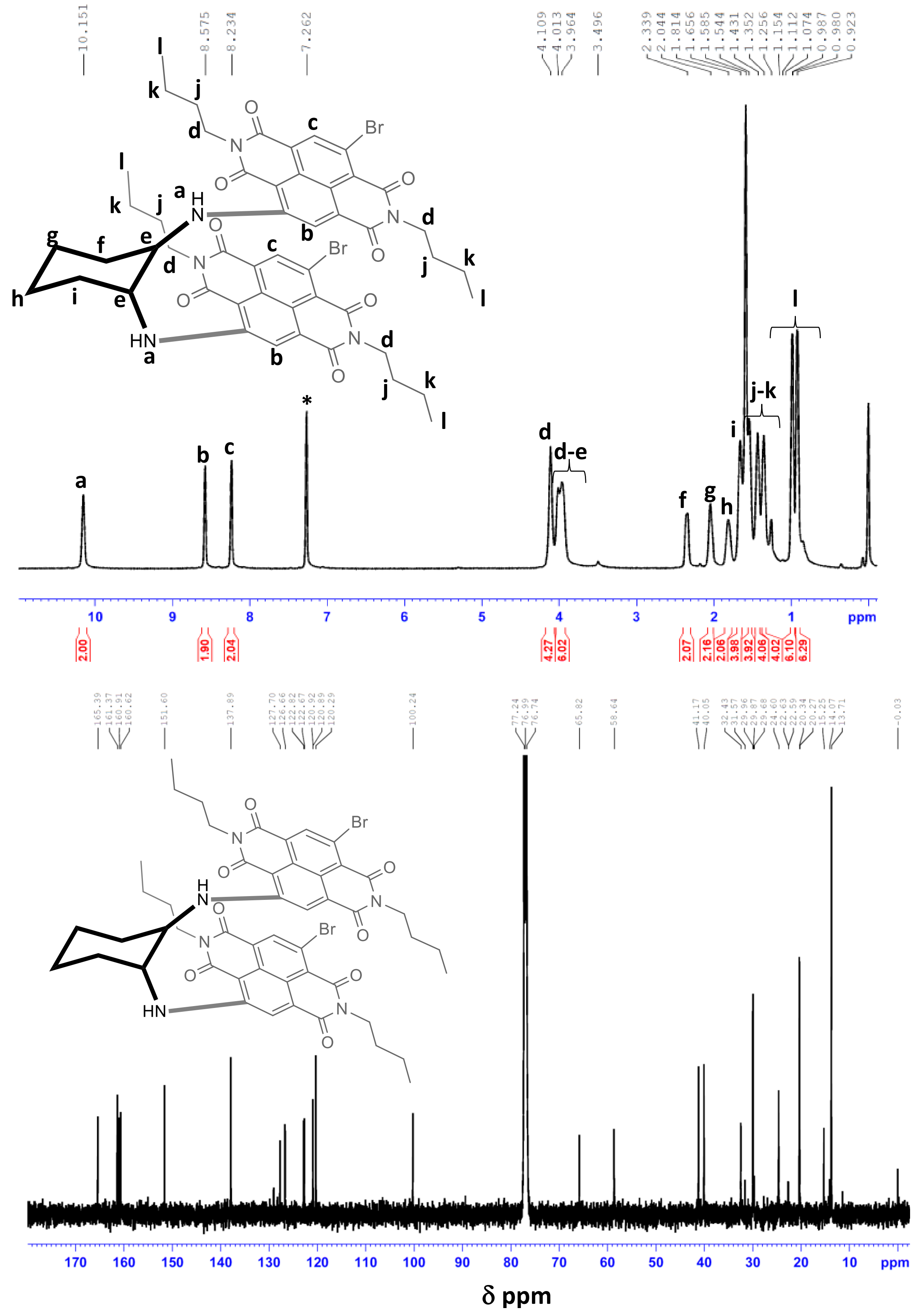

Figure S1. 500 MHz ^{1}H NMR (top) and 125 MHz ^{13}C (bottom) spectra of **PP-Clip** in $CDCl_3$ at room temperature. * represents residual solvent, H_2O peaks.

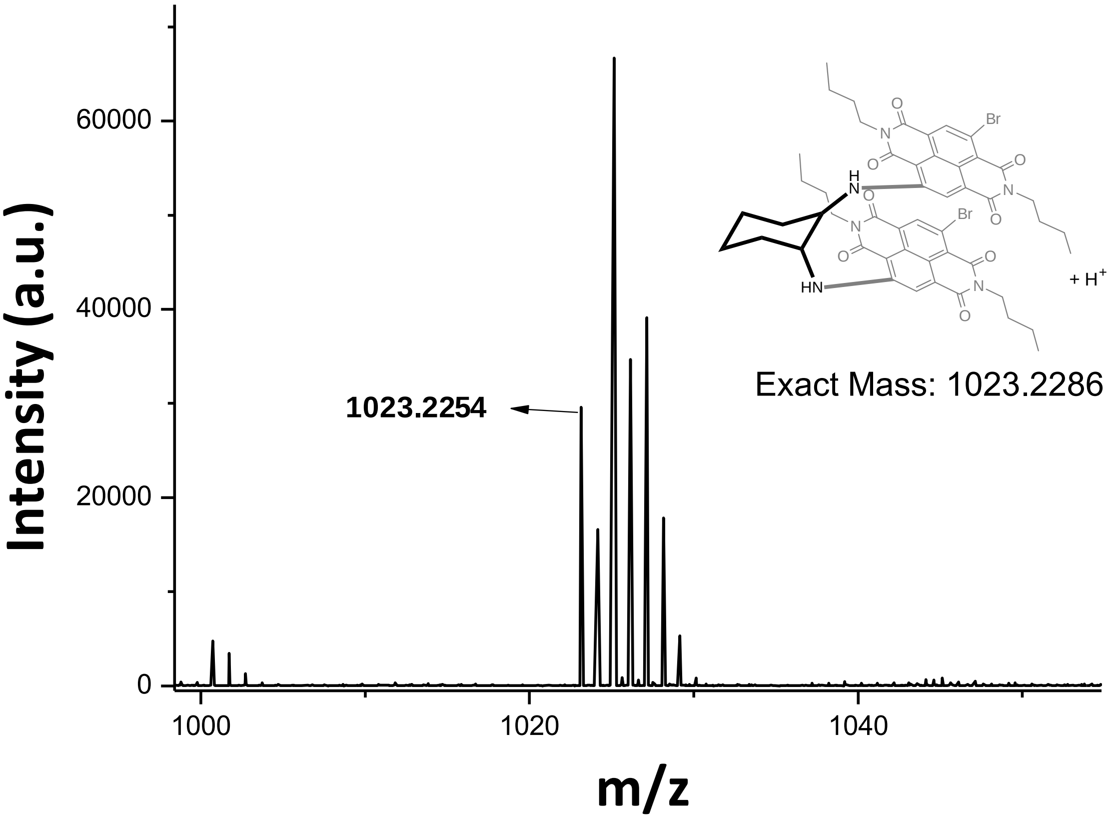

Figure S2. High-resolution mass spectrum of **PP-Clip** recorded in $CHCl_3$.

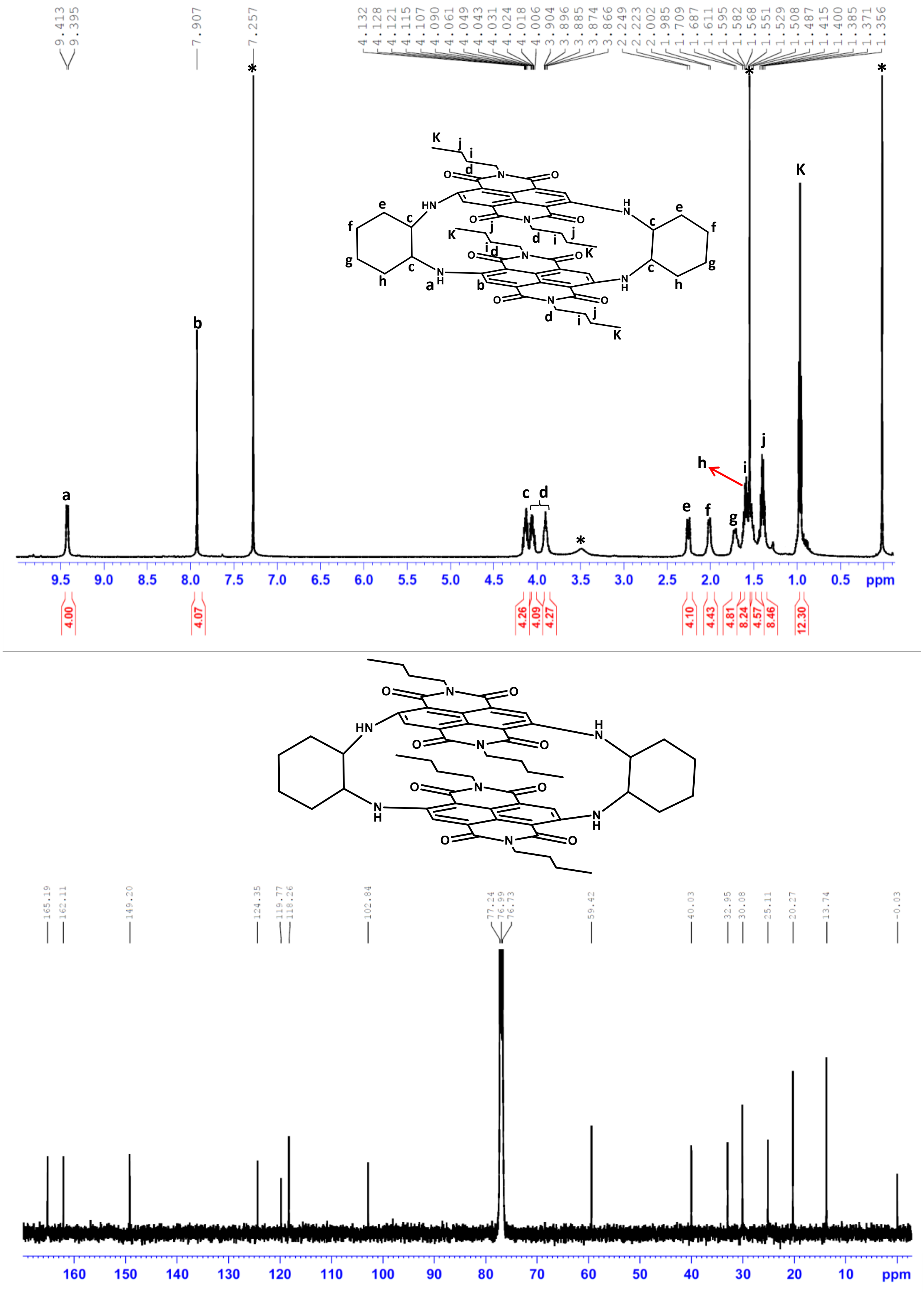

Figure S3. 500 MHz ^{1}H NMR (top) and 125 MHz ^{13}C (bottom) spectra of **PPD** in $CDCl_3$ at room temperature. * represents residual solvent, H_2O peaks.

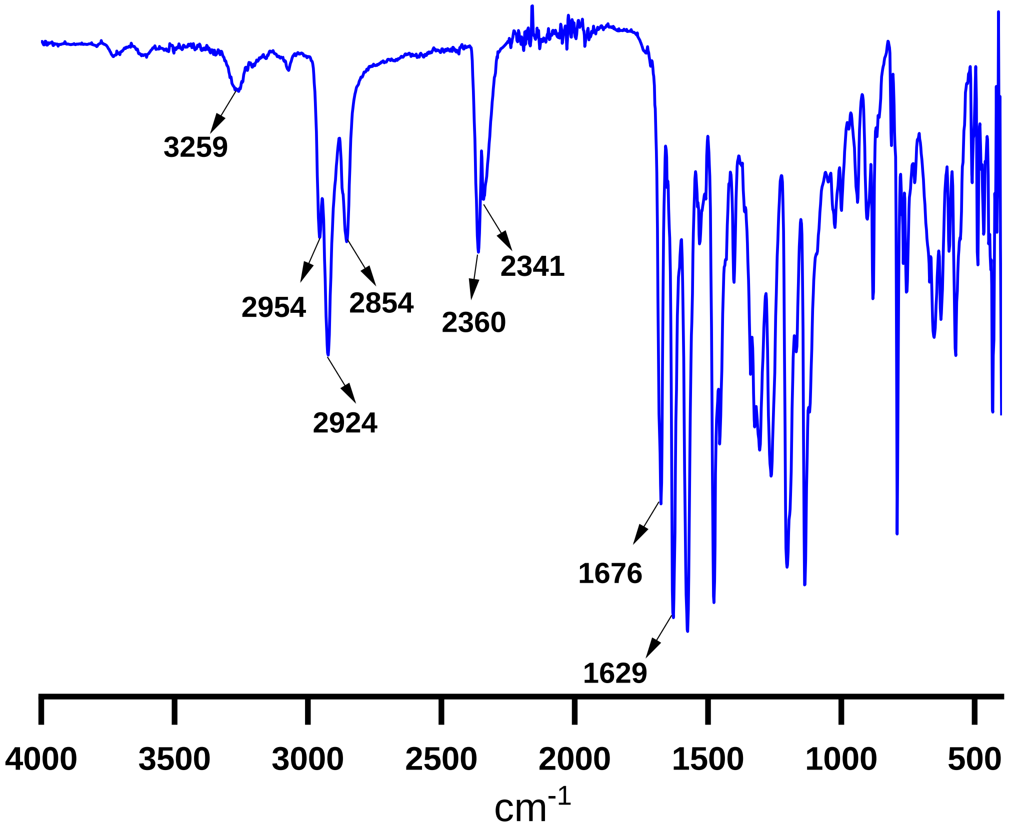

Figure S4. FTIR spectrum of **PPD**.

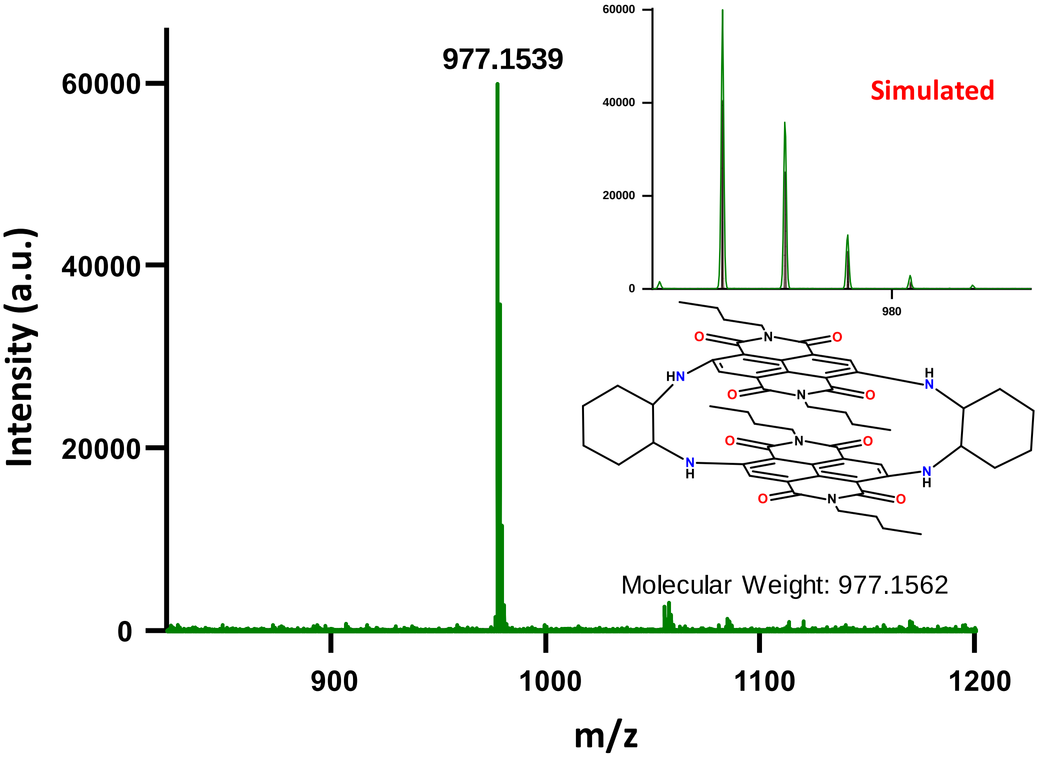

Figure S5. High resolution mass spectrum of **PPD** recorded in $CHCl_3$. Inset: Overlapping pattern of Molecular ion peak (green traces) with simulated pattern (black traces) generated using ChemCalc online program.

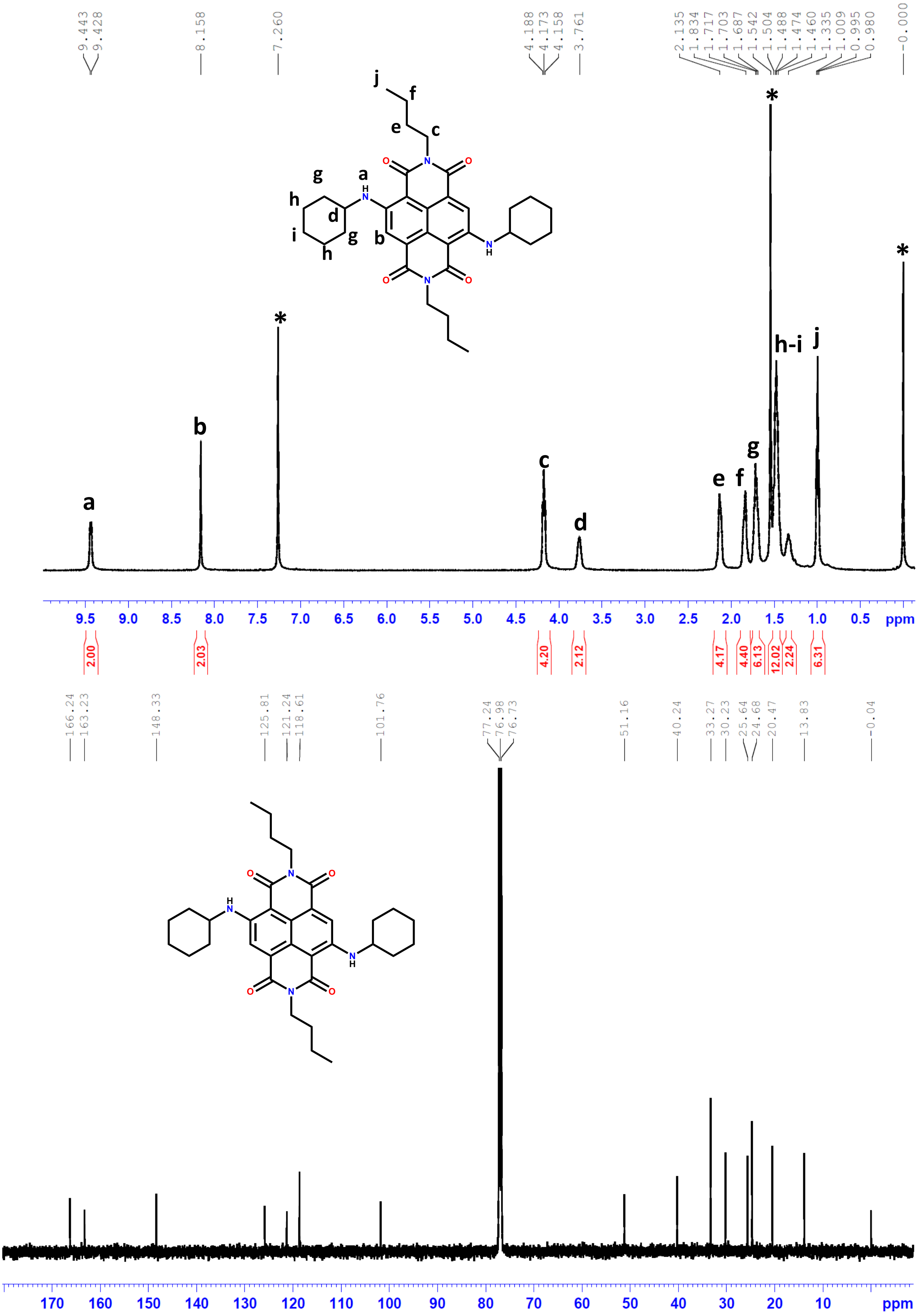

Figure S6. 500 MHz ^{1}H NMR (top) and 125 MHz ^{13}C (bottom) spectra of **PP-NDI** in $CDCl_3$ at room temperature. * represents residual solvent, H_2O peaks.

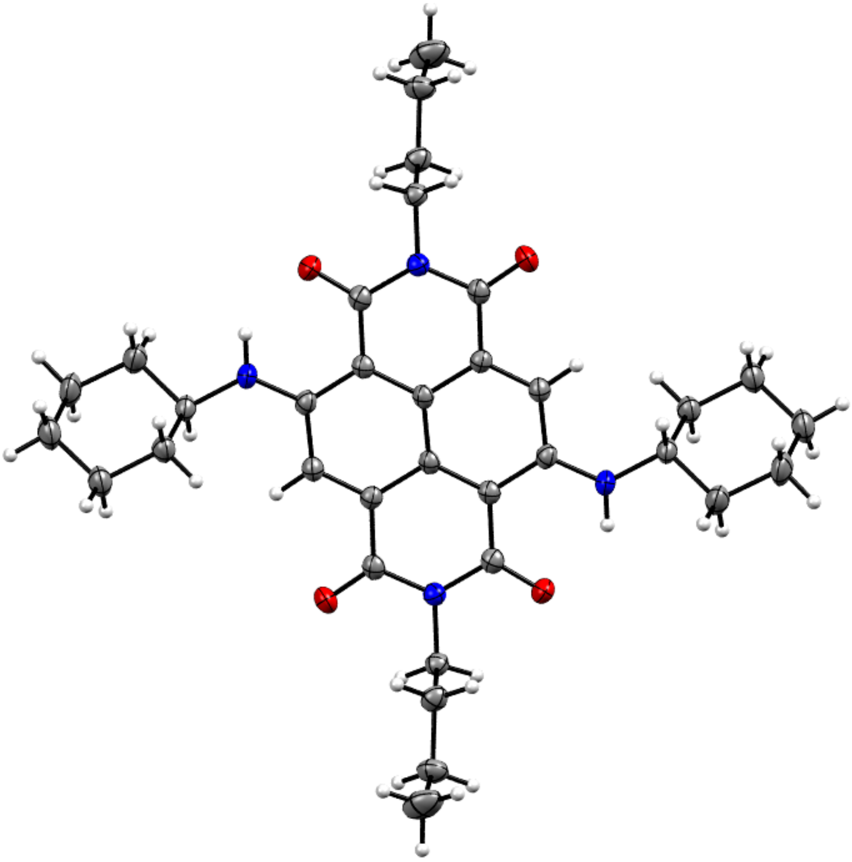

Figure S7. Ellipsoidal representation for the crystal structure of **PP-NDI**. Ellipsoids are drawn at 30% probability levels.

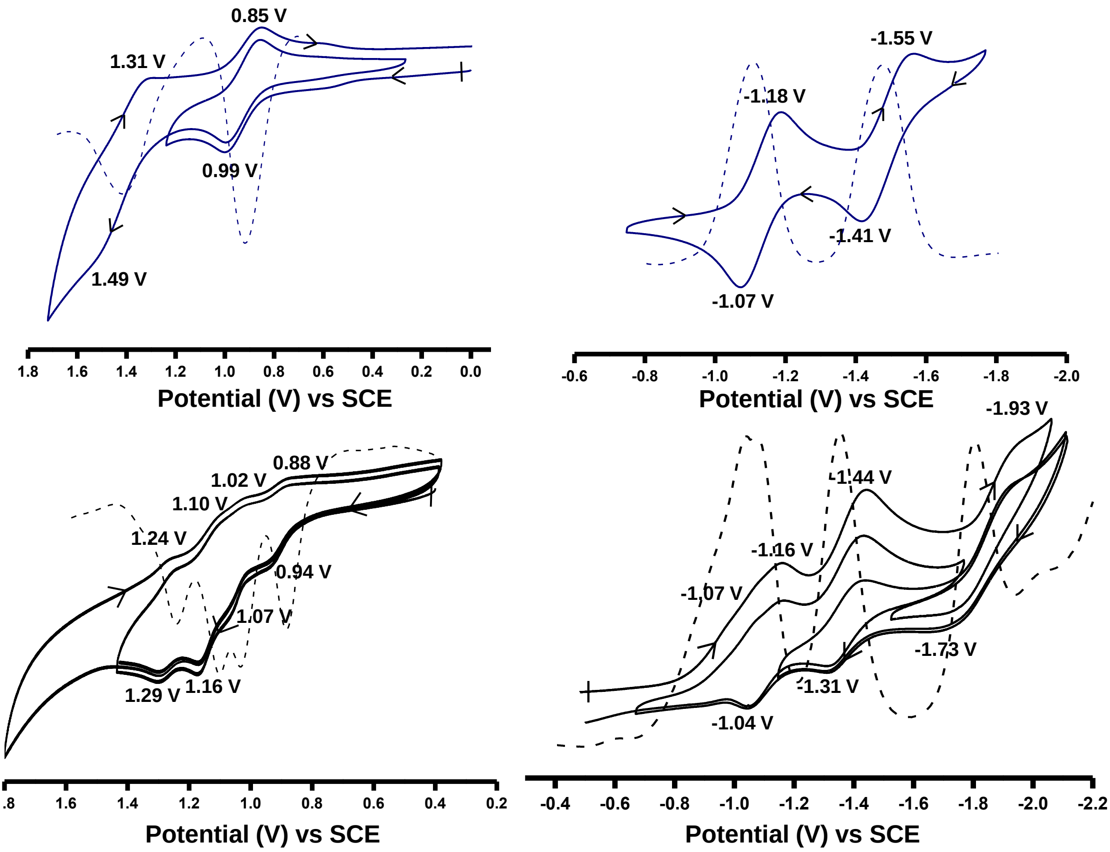

Figure S8. Cyclic and Differential Pulse (dotted line) voltammogram of molecule **PP-NDI** (Top) and **PPD** (bottom). Condition: 1 mM solution of either **PP-NDI** or **PPD** in DCM; 0.1 M Bu_4NPF_6 at 298 K; scan rate, 200 mV/s.

PPD exhibits four reductive and four oxidative redox responses. The four reductive redox signal $(E^{\text{red1-red4}})_{1/2}$ were observed at -1.04 V, -1.08 V, -1.37 V and -1.83 V, respectively. The first two closely positioned reduction potential could be identified only with the DPV. On the other hand, four closely placed oxidative redox signal $(E^{\text{ox1-ox4}})_{1/2}$ were observed at = 0.91 V, 1.04 V, 1.13 V and 1.26 V, respectively. This is in contrast to the electrochemical behavior of **PP-NDI** where only two reductive redox signals at $E^{\text{red1}}_{1/2}$ = -1.12 V and $E^{\text{red2}}_{1/2}$ = -1.48 V and two oxidative redox responses at $E^{\text{ox1}}_{1/2}$ = 0.92 V and $E^{\text{ox2}}_{1/2}$ =1.41 V were obtained. Interestingly, as the consequence of through-space electronic delocalization, the first and the fourth oxidation in **PPD** is shifted by ca. 50 mV and 200 mV, respectively towards less positive side of voltammogram. Whereas, the last reduction wave at -1.93 V was shifted towards more negative potential by ca. 400 mV to that of **PP-NDI** suggesting increased electron loading in **PPD** and also strong electronic communication between the two closely oriented NDIs.

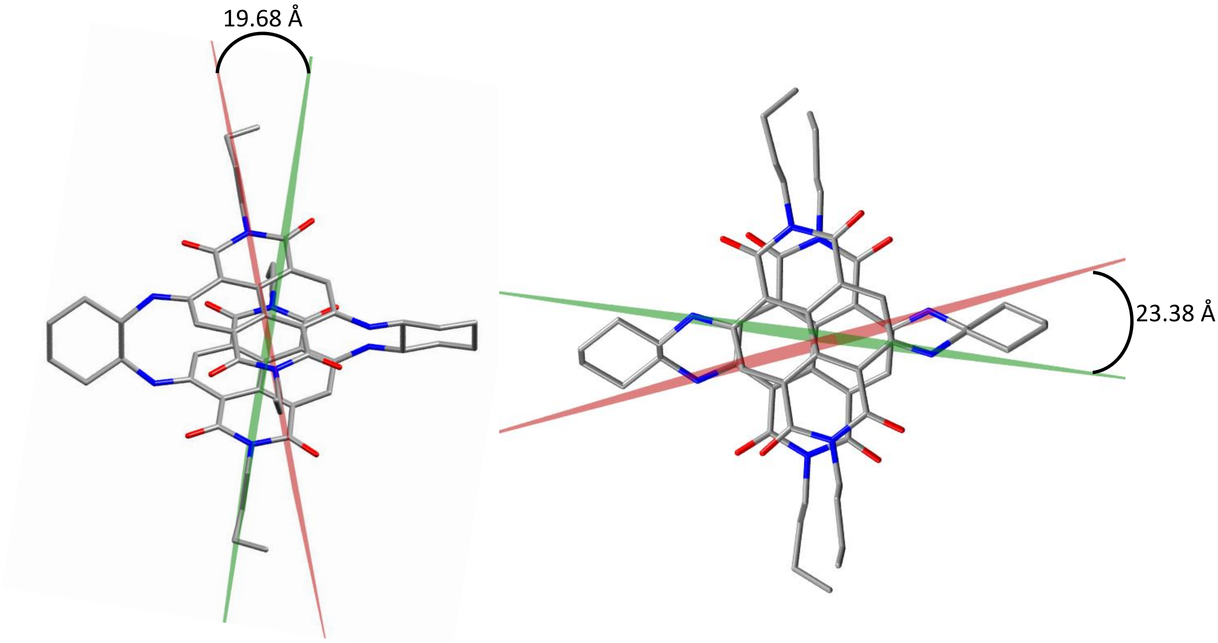

Figure S9. Representation of long- and short-axis planes in **PPD** used to calculate the angle of distortion.

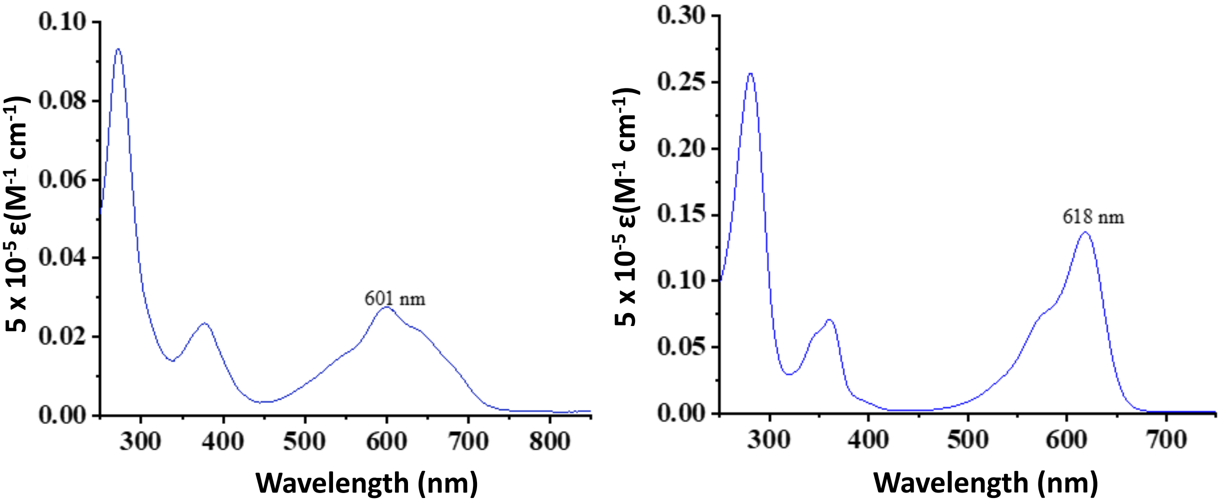

Figure S10. Absorption spectra of **PPD** (left) and reference molecule **PP-NDI** (right) in DCM solvent.

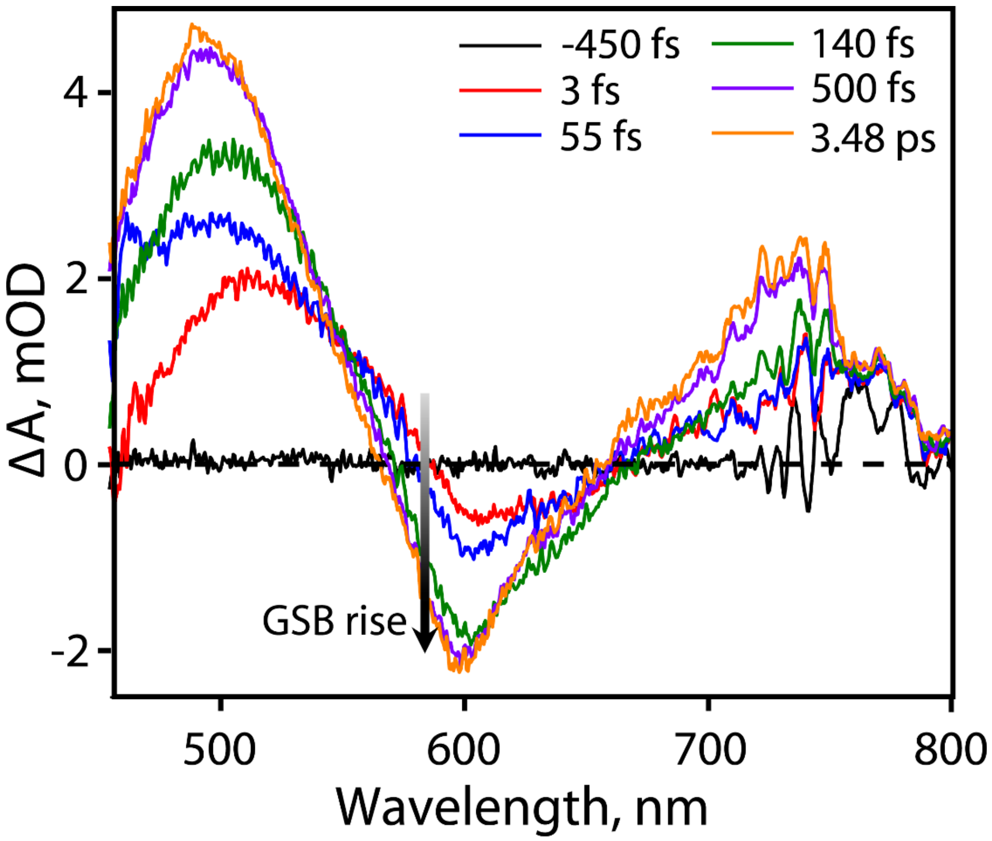

Figure S11. Transient absorption of PPD (100 μM in ACN:DCM (1:1)) subsequent to 400 nm photoexcitation showing the initial TA dynamics from -450 fs to 3.48 ps. Here the rise in the GSB feature can be clearly seen up to few picoseconds timescale in the range of 565 nm to 615 nm spectral region.

Analysis of Monomer Femtosecond Transient Absorption:

The excited state dynamics of NDI monomer (**PP-NDI**) was examined first to investigate singlet fission mechanism in NDI dimer as a control. The transient measurement was done in 200 µM of monomer solution in DCM subsequent to 620 nm photo-excitation. Figure S1 represents the key results obtained from monomer transient absorption. The transient spectra show a broad excited state absorption (ESA) feature in 430 nm to 575 nm region and another ESA feature in 730 nm to 830 nm region. Along with that there is a stimulated emission (SE) feature convoluted with ground state bleach (GSB) signal in the region of 590 nm to 700 nm. The excited state dynamics shows a bright emissive state with a lifetime of ~9.9 ns (kinetic fits shown in Figure S12) similar to our TCSPC measurement, where emission lifetime was ~11 ns in the monomer. It is also important to note here that there is no signature of triplet formation in the transient data. We discard any possibilities of singlet fission in **PP-NDI** as we do not see any triplet state spectral signature and it is energetically unfavorable.

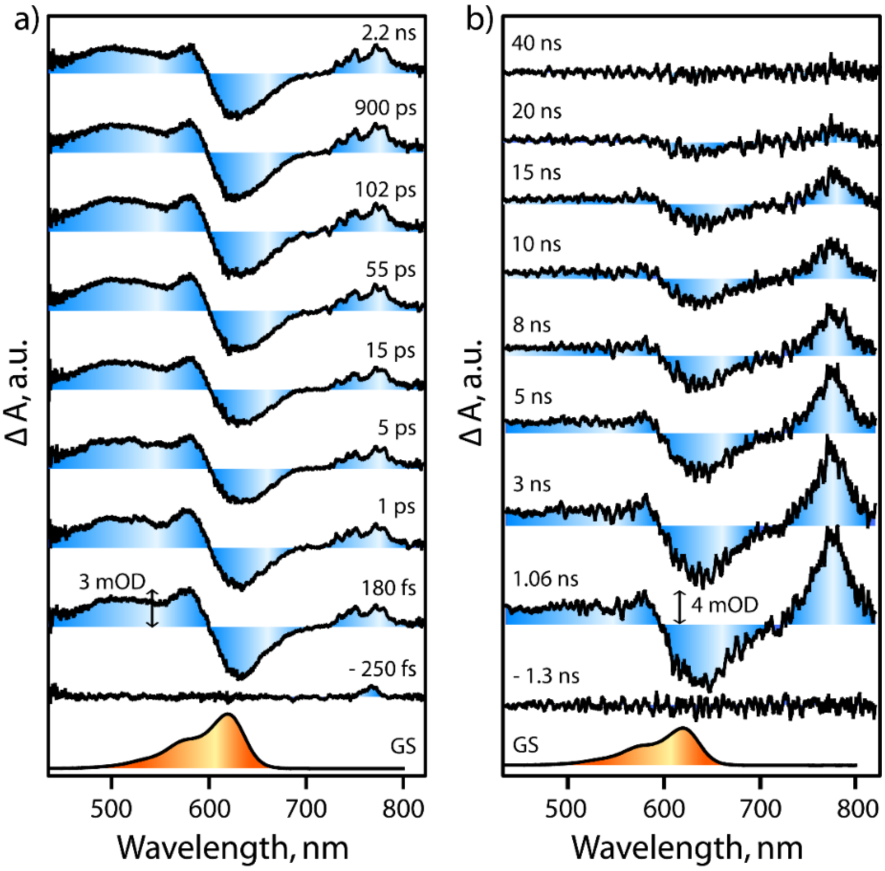

Figure S12. Broadband transient absorption of **PP-NDI** in DCM (200 µM) subsequent to 620 nm photo-excitation (20 nJ/pulse energy). (a) In femtoseconds to nanoseconds region. (b) In nanoseconds to microseconds region.

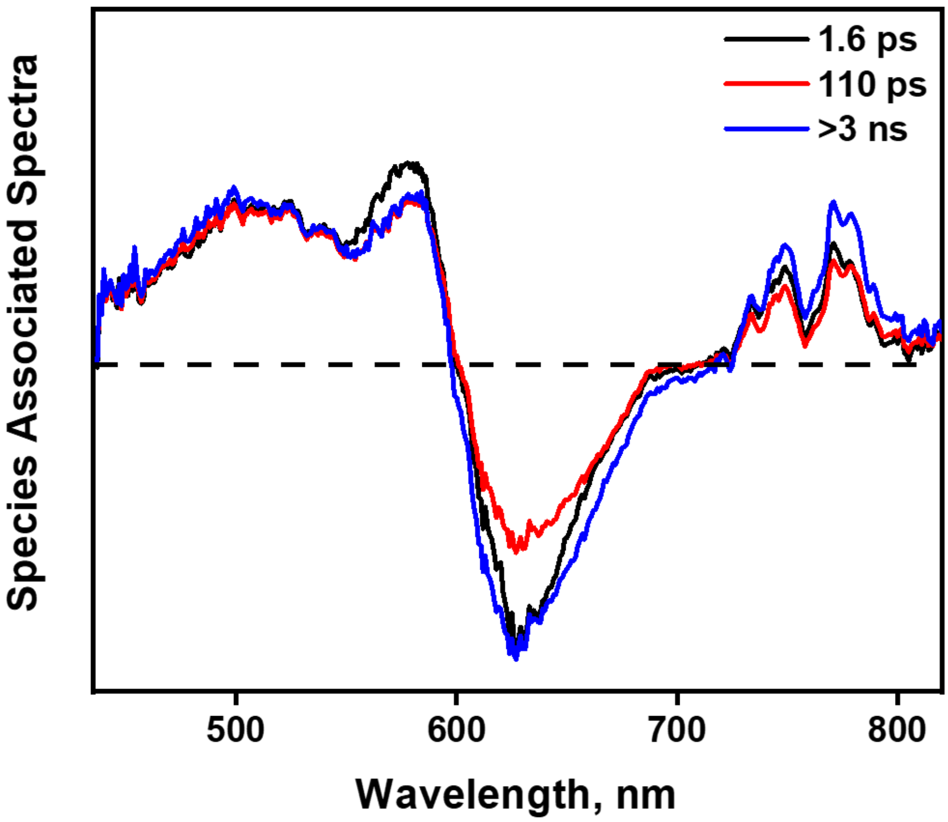

Figure S13. Species Associated Spectra of transient absorption of **PP-NDI** in DCM (200 μM) subsequent to 620 nm photo-excitation (20 nJ/pulse energy) with 3 component sequential model.

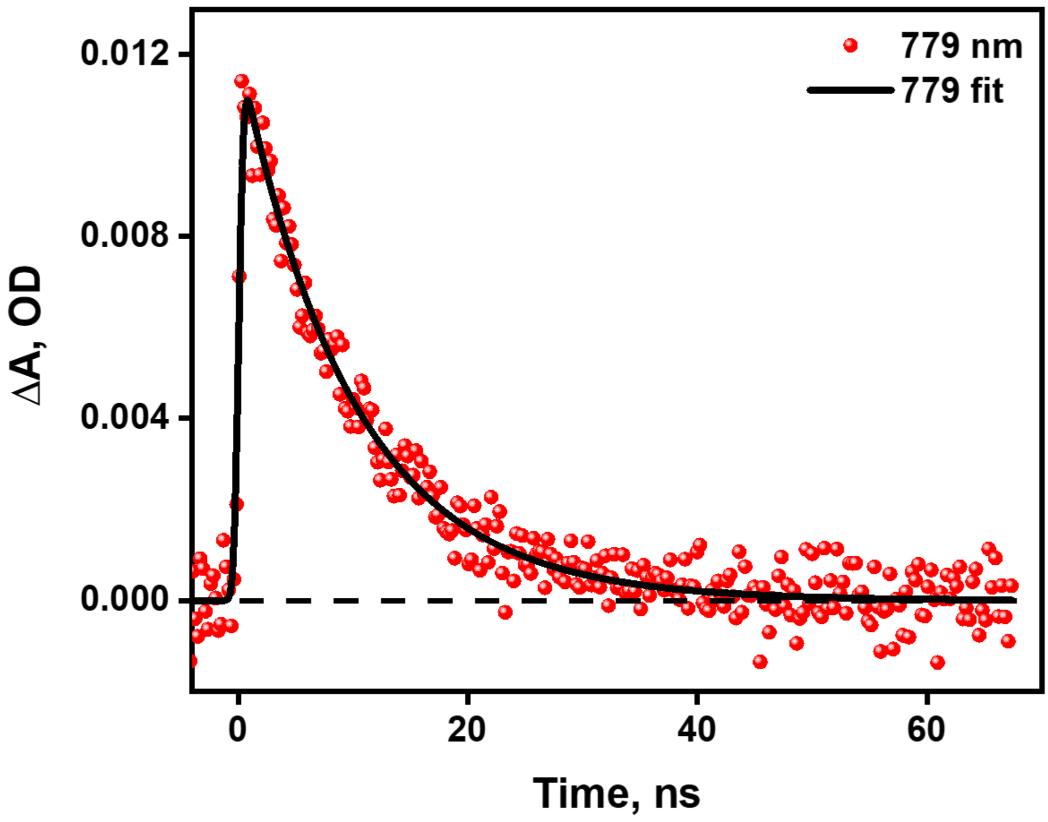

Figure S14. Single point kinetics of nanoseconds to microseconds transient absorption of **PP-NDI** in DCM (200 μM) subsequent to 620 nm photo-excitation (20 nJ/pulse energy) fitted with a mono-exponential decay of 9.9 ns lifetime.

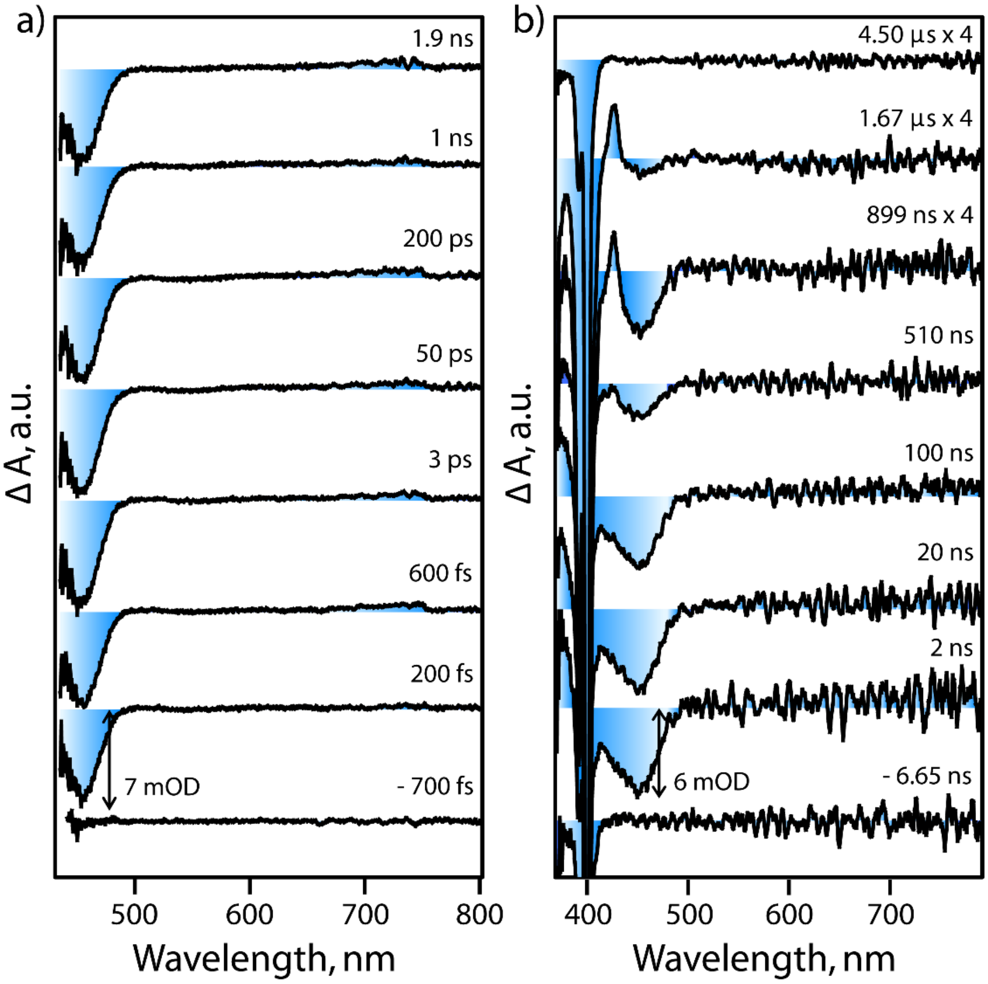

Figure S15. Broadband transient absorption of [Ru-tris(bipy)$_3$]$^{2+}$ complex (200 µM) in ACN:DCM (1:1) subsequent to 400 nm photo-excitation (400 nJ/pulse energy). (a) In femtoseconds to nanoseconds region. (b) In nanoseconds to microseconds region.

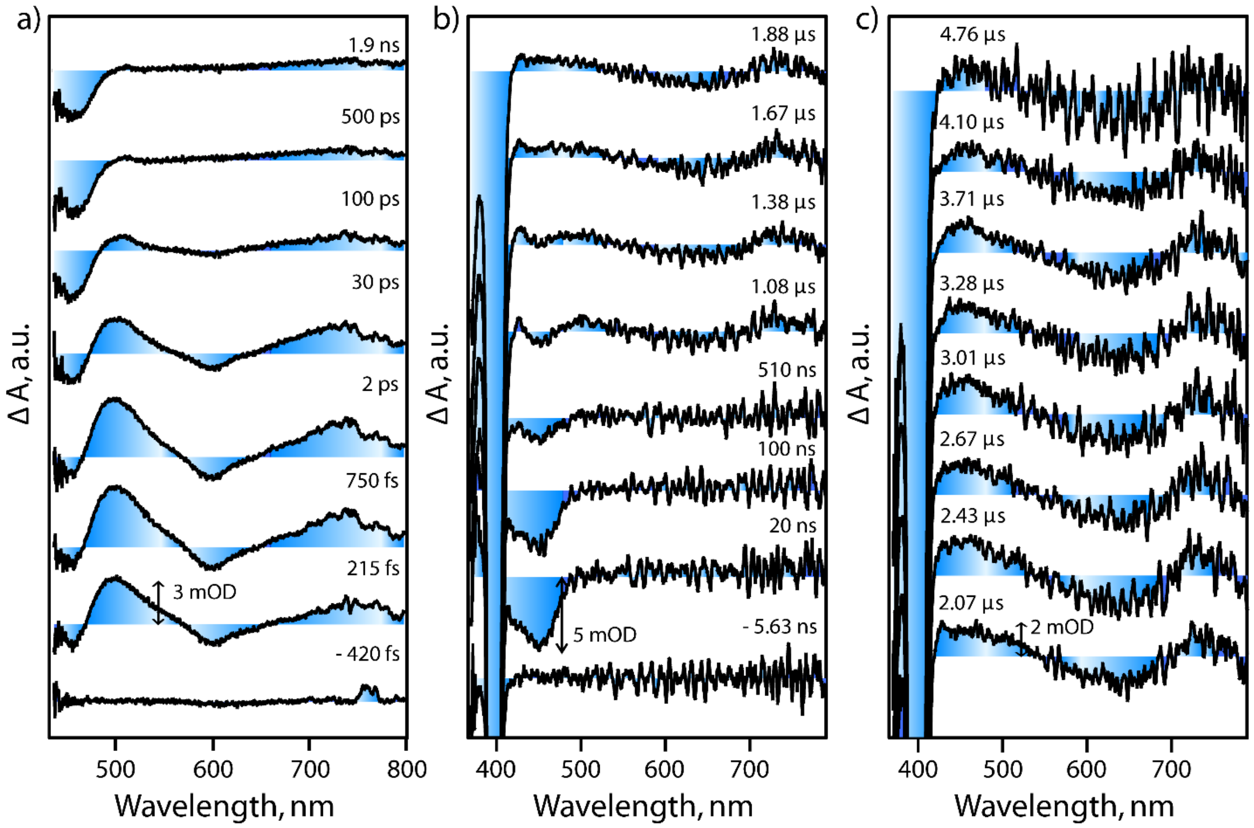

Figure S16. Broadband transient absorption for 1:2 mixtures of **PPD** (100 μM) and [Ru-tris(bipy)$_3$]$^{2+}$ complex (200 μM) in ACN:DCM (1:1) subsequent to 400 nm photo-excitation (400 nJ/pulse energy). (a) In femtoseconds to nanoseconds region. (b) and (c) In nanoseconds to microseconds region. The initial TA spectrum (up to 100 ps, figure a) in the sensitization measurement shows the SF induced triplet signature in PPD via direct excitation at 400 nm photo-excitation and a convoluted feature of the sensitizer TA. On the later timescale (ns to μs, figure b and c) we do observe the sensitizer transient signature first and then the sensitized triplet spectrum (via ISC) of the PPD appears in the 1 μs to 4.75 μs.

In the sensitization experiment after photoexcitation at 400 nm at [Ru-tris(bipy)$_3$]$^{2+}$ complex absorption band we see a mixed signature of both the ESA feature from the complex as well as the SF generated T-T pair signature from the direct photoexcitation of small fraction of the PPD molecule. Then within hundreds of picoseconds the SF induced T-T signature of PPD goes away and the transient spectra is exclusively dominated by the Ru-complex transient features as observed in Figure S15a and S15b. Interestingly in the nanoseconds to microseconds temporal region of the transient spectra we could observed the clear signature of sensitized triplet state spectra of PPD and the triplet state spectral features of the Ru-complex (shown in Figure S14) disappeared quickly. In the sensitized triplet spectrum, the ESA features between 450 nm to 525 nm and 700 nm to 750 nm matches well with the T-T pair spectra for the PPD direct photoexcitation at 400 nm.

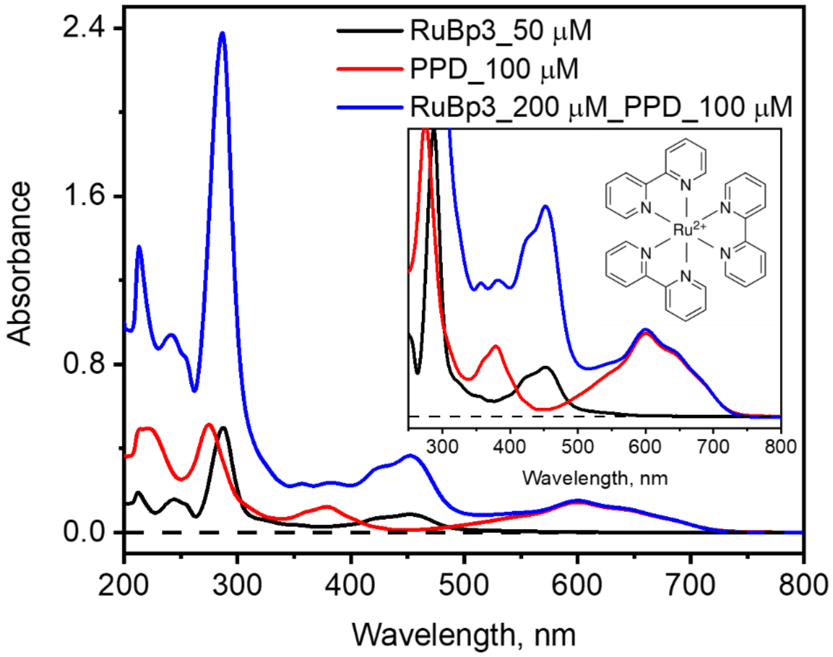

Figure S17. Steady state absorption of NDI dimer **PPD** (RR isomer) solution (100 μM), in ACN:DCM (1:1), the sensitizer, $[\text{Ru-tris(bipy)}_3]^{2+}$ complex (50 μM) in ACN:DCM (1:1) and 1:2 mixtures of **PPD** (100 μM) and $[\text{Ru-tris(bipy)}_3]^{2+}$ complex (200 μM) in ACN:DCM (1:1). (Inset: Structure of $[\text{Ru-tris(bipy)}_3]^{2+}$ complex.)

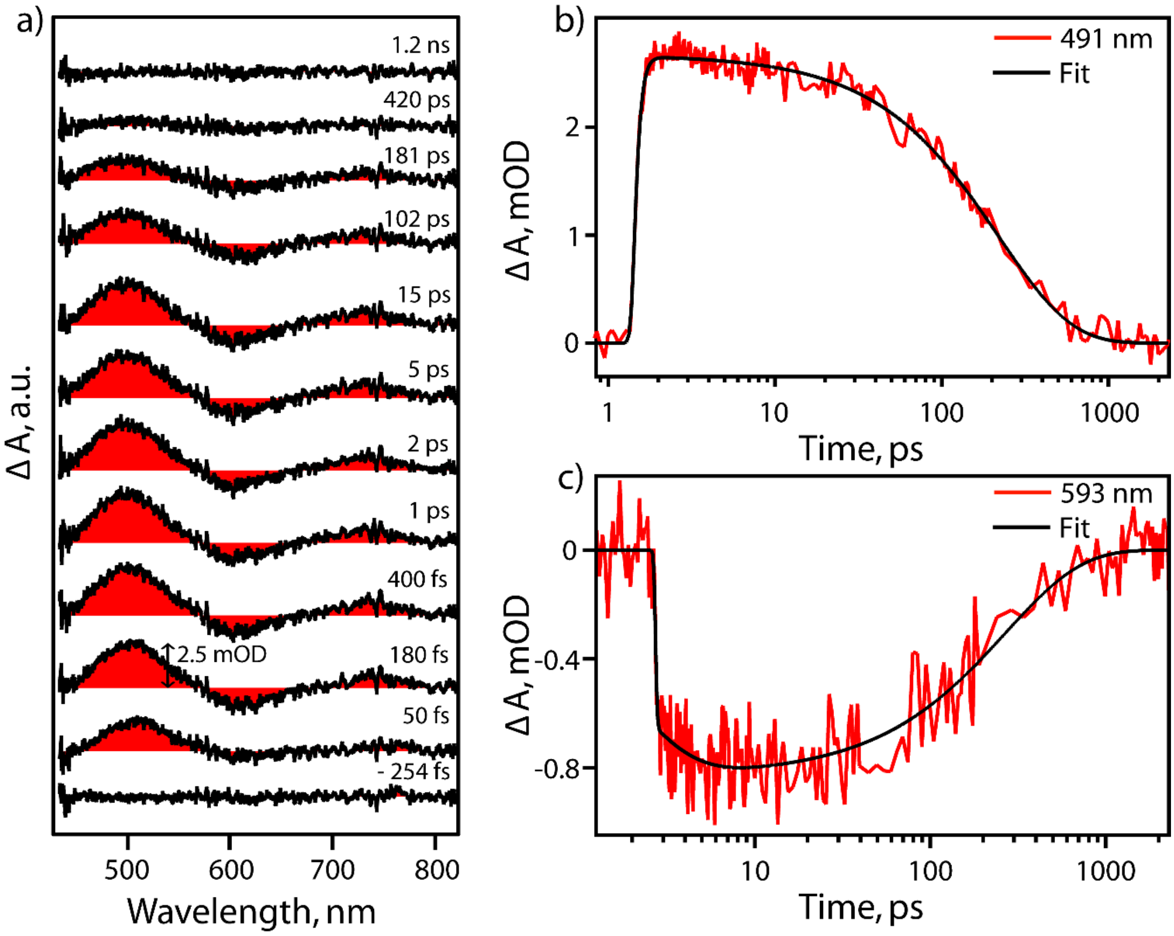

Figure S18. (a) Transient absorption of PPD (200 µM in DCM) subsequent to 620 nm photoexcitation. (b), (c) Single point kinetics at 491 nm (T-T pair) and 593 nm (GSB) respectively.

The 491 nm kinetics shows a rise time of 103 ± 16 fs and a decay of 220.5 ± 11.8 ps. On the other hand, the kinetics at 593 nm for the GSB shows a rise time of 1.5 ± 1.1 ps and a decay of 268 ± 50 ps. For the 620 nm pump excitation we observed the same result as obtained for 400 nm excitation at π -π* band. The spectral features and the position are exactly same as observed for both 400 nm and 620 nm excitation. The SF dynamics is similar for 620 nm excitation where we observed SF happens by less than a picosecond timescale and the TT pair has a lifetime of ~220 ps. It is to be noted here that the TT pair lifetime for 620 nm excitation is slightly higher compared to 400 nm excitation (~70 ps). The pump energy used for 620 nm excitation was 20 nJ/pulse.

Computational Details:

The NDI monomers in the dimer of crystallographic structure consist with four nitrogen atoms, two of them are connected with an alkene (1,3-diene) moiety and other two are connected with cyclohexane moiety. To reduce the computational cost, we have substituted the alkene group by a methyl group and cyclohexane group by an ethane group. Both structures are shown in Figure S17 of Supporting Information. The optimization is carried out by using B3LYP functional and 6-31+G(d,p) Pople basis set. We have also incorporated the Grimme's D3 dispersion correction to the B3LYP functional. Gaussian16 (Revision B.01) program was used to optimize the structure.[2] We have performed state-averaged complete active space self-consistent field (SA-CASSCF) method alongwith the extended multiconfigurational quasidegenerate perturbation theory of second order (XMCQDPT2) to calculate the low-lying singlet and triplet excited states.[3-4] An equal weightage of three roots (SA3) was considered for SA-CASSCF(*n*e,*m*o) calculations, where *n* is the number of active electrons (e) and *m* is the number of active orbitals (o). The active orbitals in SA-CAS calculations are chosen by investigating their energy levels.[5] A double-ζ valance (DZV) basis set is applied to reduce the computational cost.[6] In this work, 4e-4o, 6e-6o, 8e-8o and 10e-10o configurations are considered in SA-CASSCF calculations. In XMCQDPT2 calculations, the conventional shifting parameter of 0.02 hartree is used to prevent the intruder effects.[7] These calculations are performed with Firefly 8.0 program.[4,8] The energies of low-lying excited singlet state are also calculated using CASSCF(12e,10o)/NEVPT2 method and def2-SVP basis set in ORCA 5.0.3.[9-10]

Choice of active space in CAS calculations:

"The active orbitals in CASSCF calculations are chosen by analyzing the degeneracy in their energies.ref The preliminary calculations were carried out in ORCA 5.0.3.[9] First, we have taken the optimized structure and performed a single-point DFT calculation with the B3LYP functional and def2-SVP basis set. The energies for the HOMO–5 to HOMO are –7.2, –7.2, –6.8, –6.8, –5.7 and –5.4 eV, respectively. Consequently, the energies of LUMO to LUMO+5 are –3.1, –3.1, –1.6, –1.5, –0.8 and –0.7 eV, respectively. Therefore, there is a 2-fold degeneracy pattern. Also, these orbitals show predominant p-character from C, N and O atoms. Next, we have carried out a CAS(12,12) calculation, where we have optimized just one singlet state. The occupation numbers, N(occ) for HOMO–5 to LUMO+5 are calculated as 1.98, 1.98, 1.96, 1.95, 1.93, 1.93, 0.07, 0.07, 0.05, 0.05, 0.03, and 0.00, respectively. Clearly, the calculation shows that the LUMOs are not strongly occupied. To improve this finding, we have taken 20 singlet roots and calculated N(occ): 1.83, 1.80, 1.86, 1.86, 1.62, 1.63, 0.40, 0.36, 0.24, 0.18, 0.18, and 0.04. These observations indicate that one can use the arrangement of 10 electrons in 10 orbitals in an SA-CASSCF calculation. However, the N(occ) for the LUMOs are not also predominant here. For fine-tuning, we have calculated the same with CAS(6,6), and the occupation numbers are 1.79, 1.56, 1.55, 0.45, 0.45, and 0.18. In this calculation, the energies for HOMO–2 to LUMO +2 are –8.9, –7.0, –7.0, –1.3, –1.3 and –1.2, respectively. A nice degeneracy between HOMO–1 and HOMO, LUMO and LUMO +1 can be observed. Therefore, we have concluded that for such systems, CAS(6,6) and CAS(4,4) are the best choices, especially CAS(4,4)."

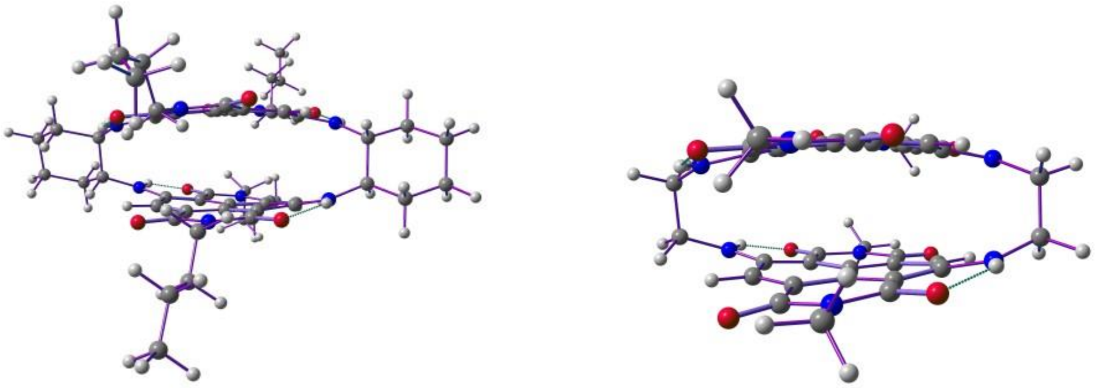

1 **2**

Figure S19: B3LYP-D3/6-31+g(d,p) optimized structures of (**1**) crystallographic **PPD** and (**2**) simplified NDI dimer (cyclohexane ring has been replaced with a ethylene linker).

Table S1: Configuration State Functions (CSFs) correspond to the S_{1a} and S_{2a} states with SA3-CASSCF(4,4)/XMCQDPT2 calculations. The corresponding spin arrangements for ME, LE and CT states are shown in the right side.

S_{1a}		
α	***β***	Coefficients
1100	1100	0.98
0110	0110	–0.06
0101	0101	–0.06
1010	1010	–0.06
0101	**1010**	**–0.05 (ME)**
1010	0101	–0.05 (ME)
S_{2a}		
α	***β***	Coefficients
1001	**1100**	**0.43 (LE)**
1100	1001	–0.43 (LE)
1100	**1010**	**0.42 (CT)**
1010	1100	–0.42 (CT)
0101	1100	0.26 (LE)
1100	0101	–0.26 (LE)
1100	0110	0.25 (LE)
0110	1100	–0.25 (LE)
0011	0110	0.06
0110	0011	–0.06
0011	0101	0.05
0101	0011	–0.05

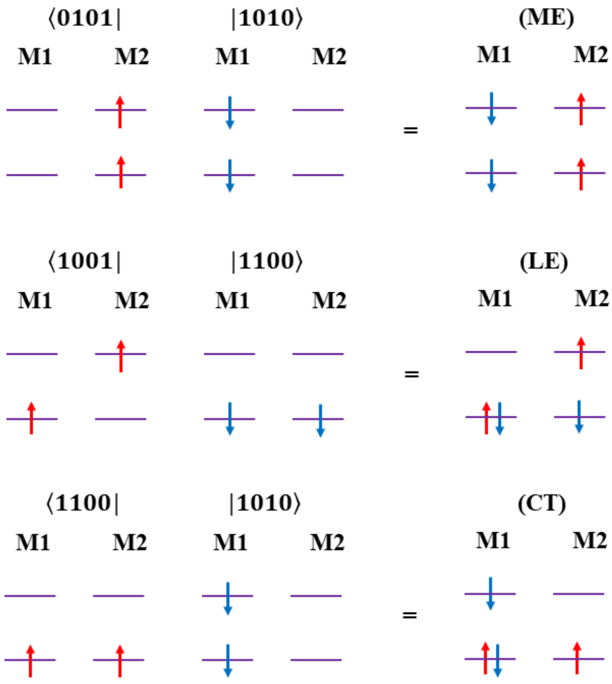

We have also carried out the calculations for the low-lying singlet excited states of the planar dimeric structure, as shown in Figure S20.

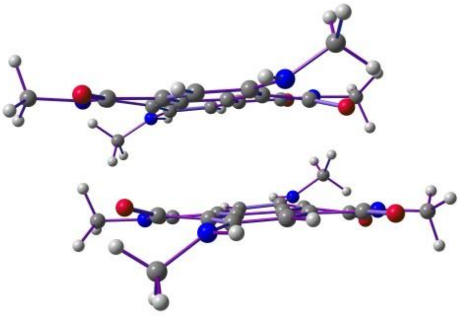

Figure S20: B3LYP-D3/6-31+g(d,p) optimized structures of the planar conformation.

Table S2: The vertical excitation energies (in eV) for the monomer (PP-NDI) and dimer (PPD) structures at TD-B3LYP//6-31+g(d,p)//DCM level. The oscillator strengths are in parentheses.

	S_1	T_1	T_2
PP-NDI	2.13 (0.22)	1.32 (0.00)	2.66 (0.00)
PPD	1.85 (0.03)	1.32 (0.00)	1.91(0.00)

Table S3: Configuration State Functions (CSFs) correspond to the S_{1a} and S_{2a} states with SA3-CASSCF(4,4)/XMCQDPT2 calculations on planar dimeric conformation.

S_{1a}		
α	***β***	Coefficients
1100	1100	0.98
1001	1001	–0.06
0110	0110	–0.06
0110	1001	–0.05
1001	**0110**	**–0.05**
S_{2a}		
α	***β***	Coefficients
1100	**1010**	**0.53 (LE)**
1010	1100	–0.53 (LE)
1100	**0101**	**0.46 (CT)**
0101	1100	–0.46 (CT)
1010	0011	0.05
0011	1010	–0.05

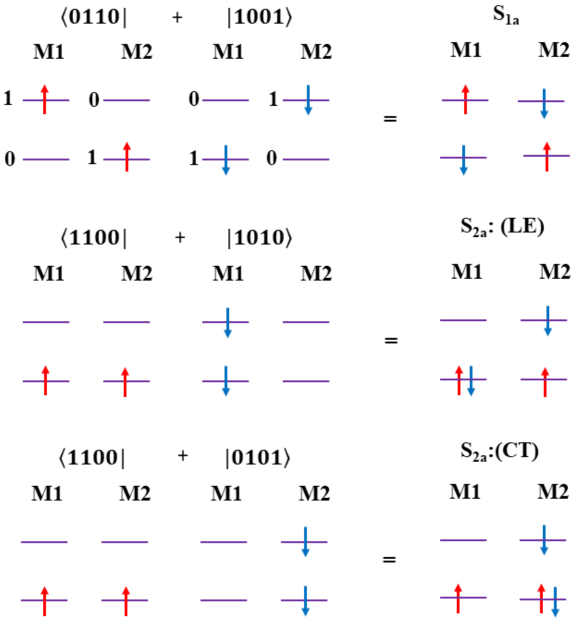

Table S4: Table compiling the previous reports on arylene diimide i.e. both PDI and TDI derivatives that have the potential to show singlet fission. For each derivative the S_1/T_1 energies of the monomers are provided along with SF timescales for those that experimentally show singlet fission.

S. No.	**π-Scaffold**	**E(S_1) (eV)**	**E(T_1)/ ^{a}E(TT) (eV)**	**ΔE**	**Timescales of SF**	**References:**
1.	PDI	2.17	^{a}1.90	Exoergic	~400 fs to 500 ps.	*J. Phys. Chem. Lett. 2015, 6, 360–365.*
2.	PDI	2.50 2.40	1.40 1.20	Endoergic Isoergic	~2.5 ps	*J. Am. Chem. Soc. 2019, 141, 13143–13147.*
3.	PDI	2.08	1.14	Endoergic	~180 ps	*J. Am. Chem. Soc. 2013, 135, 14701–14712.*
4.	PDI	2.34	1.20	Endoergic	Not determined	*J. Phys. Chem. 1987, 91, 6373.*
5.	PDI	2.09	1.1	Endoergic	~3.8 ns	*J. Phys. Chem. Lett. 2016, 7, 4922–4928.*
6.	TDI	1.87	0.77	Exoergic	~300 fs to 8 ns.	*Chem. Mater. 2006, 18, 3715–3725. Nat. Chem. 2016, 8, 1120–1225.*
7.	TDI	1.84	0.86	Exoergic	~12 ps	*J. Chem. Phys. 2020, 153, 244306.*
8.	TDI	1.77	0.77	Exoergic	~3 ps to ~30 ps	*J. Am. Chem. Soc. 2017, 139, 663–671*

B3LYP-D3/6-31+g(d,p) optimized coordinates of structure 2 of Figure S17:

7	-3.378770245	0.408230030	1.799350130
7	3.568090258	-0.423800031	1.665770121
7	0.983960071	-3.774770273	1.183690086
6	-0.602780044	0.115160008	1.740160126
6	-1.138210082	1.398750101	1.677870122
6	-0.311470023	2.517080182	1.525100110
6	-1.420890103	-1.009580073	1.749820127
6	1.625930118	1.045580076	1.725010125
6	-0.072410005	4.926070357	0.772520056
8	-3.169830230	2.646850192	1.687200122
6	0.798960058	-0.103860008	1.709950124
7	-0.765890055	3.744790271	1.271830092
6	-0.904060065	-2.283820165	1.646320119
1	-1.608130116	-3.102470225	1.611270117
6	-2.860940207	-0.885960064	1.813070131
6	0.486950035	-2.496050181	1.482010107
6	1.316870095	-1.408020102	1.623200118
8	3.359450243	-2.640510191	1.422870103
6	-2.591460188	1.577490114	1.722170125
8	-3.619190262	-1.827550132	1.873940136
6	1.106180080	2.306550167	1.624270118
1	1.796130130	3.139340227	1.589460115
8	3.864870280	1.815500132	1.936960140
6	2.777440201	-1.547810112	1.538240111
6	0.139860010	-4.903140355	0.742650054
6	-4.841870351	0.552320040	1.891170137
1	-5.191700376	1.187490086	1.075370078
1	-5.282500383	-0.437650032	1.833610133
6	3.106700225	0.895130065	1.785560129
6	5.057000366	-0.613870044	1.576450114
1	5.277530382	-1.180230085	0.671630049
1	5.512240399	0.371600027	1.558880113
1	1.996220145	-3.828670277	1.105700080
1	-1.782720129	3.807750276	1.293330094
1	0.915270066	5.017200363	1.234050089
1	-0.792460057	-4.923410357	1.312190095
7	3.379570245	0.406290029	-1.799210130
7	-3.567910258	-0.421960031	-1.665580121
7	-0.987480072	-3.774110273	-1.183550086
6	0.603100044	0.114590008	-1.740670126
6	1.139750083	1.398500101	-1.677800122
6	0.313840023	2.516040182	-1.525110110
6	1.420360103	-1.010760073	-1.750250127
6	-1.625850118	1.046680076	-1.725200125
6	0.076580006	4.925260357	-0.772700056
8	3.172030230	2.644370192	-1.687880122
6	-0.798540058	-0.102680007	-1.709790124
7	0.769170056	3.743420271	-1.271920092

6	0.901930065	-2.285320166	-1.645630119
1	1.605220116	-3.104550225	-1.610070117
6	2.860770207	-0.887520064	-1.812850131
6	-0.489510035	-2.495790181	-1.481950107
6	-1.318350095	-1.407850102	-1.622570118
8	-3.361190243	-2.638100191	-1.423180103
6	2.593400188	1.575440114	-1.721460125
8	3.617130262	-1.830380133	-1.873930136
6	-1.105160080	2.307260167	-1.624550118
1	-1.793880130	3.141030227	-1.590040115
8	-3.863950280	1.817550132	-1.936540140
6	-2.778370201	-1.545840112	-1.538630111
6	-0.144220010	-4.903090355	-0.742440054
6	4.841850351	0.549290040	-1.890670137
1	5.194570376	1.171800085	-1.066250077
1	5.281090383	-0.442080032	-1.847970134
6	-3.105810225	0.897330065	-1.786120129
6	-5.057230366	-0.610200044	-1.576900114
1	-5.278320382	-1.180350086	-0.674640049
1	-5.511000399	0.375830027	-1.554810113
1	-1.999810145	-3.827240277	-1.105780080
1	1.786050129	3.805740276	-1.293500094
1	-0.911160066	5.016820363	-1.234020089
1	0.788050057	-4.924300357	-1.312020095
1	-5.105880370	1.031390075	2.837610206
1	-5.400780391	-1.175030085	-2.445220177
1	5.105260370	1.042170076	-2.830100205
1	5.399460391	-1.183180086	2.442230177
1	0.681240049	-5.821630422	0.999380072
1	-0.686360050	-5.821180422	-0.998970072
1	-0.652400047	5.803180420	1.075740078
1	0.656940048	5.801880420	-1.076700078

B3LYP-D3/6-31+g(d,p) optimized coordinates of planar dimer structure of Figure S18:

7	-4.518770327	0.558910040	-0.873490063
7	2.300270167	-0.564040041	-2.307140167
7	0.630840046	3.524370255	-1.949480141
6	-1.783820129	0.078570006	-1.383940100
6	-2.662470193	-1.035380075	-1.219730088
6	-2.135880155	-2.351520170	-1.279640093
6	-2.263750164	1.409120102	-1.236980090
6	0.062150005	-1.411860102	-1.863400135
8	-4.974660360	-1.615720117	-1.330610096
6	-0.411050030	-0.080920006	-1.701040123
7	-2.796980203	-3.518070255	-1.001230073
6	-1.423990103	2.482230180	-1.394410101
1	-1.851820134	3.472860252	-1.271880092

6	-3.695150268	1.681370122	-0.949350069
6	-0.049870004	2.346840170	-1.742660126
6	0.469520034	1.033300075	-1.853320134
8	2.790690202	1.594440116	-1.839420133
6	-4.109790298	-0.763020055	-1.143820083
8	-4.141560300	2.816430204	-0.832170060
6	-0.768240056	-2.486910180	-1.658420120
1	-0.338750025	-3.479410252	-1.761570128
8	1.908880138	-2.816790204	-2.402950174
6	1.906470138	0.756500055	-1.997210145
6	-5.957840432	0.773160056	-0.678710049
1	-6.351430460	-0.020790001	-0.043940003
1	-6.091820441	1.748090127	-0.215550016
6	1.475980107	-1.680930122	-2.217850161
6	3.729770270	-0.760420055	-2.581650187
1	4.312450312	-0.651730047	-1.664020121
1	3.860560280	-1.758450127	-2.993230217
7	4.518550327	0.557810040	0.873810063
7	-2.300030167	-0.568850041	2.306700167
7	-0.632040046	3.520590255	1.952900141
6	1.783770129	0.076160006	1.383980100
6	2.662770193	-1.037340075	1.218500088
6	2.136540155	-2.353680171	1.276740092
6	2.263320164	1.407010102	1.238710090
6	-0.061710004	-1.415430103	1.861730135
8	4.975040360	-1.617020117	1.330280096
6	0.411030030	-0.084140006	1.700820123
7	2.798030203	-3.519560255	0.996530072
6	1.423220103	2.479680180	1.397280101
1	1.850790134	3.470570251	1.276010092
6	3.694690268	1.679940122	0.951640069
6	0.049060004	2.343460170	1.745060126
6	-0.469910034	1.029630075	1.854280134
8	-2.791310202	1.589870115	1.841090133
6	4.110050298	-0.764470055	1.143390083
8	4.141110300	2.815230204	0.836700061
6	0.769010056	-2.489990180	1.655490120
1	0.339860025	-3.482750252	1.757570127
8	-1.907860138	-2.821590204	2.400010174
6	-1.906740138	0.752160054	1.998030145
6	5.957430432	0.773400056	0.679210049
1	6.352800460	-0.023580002	0.049450004
1	6.090270441	1.745940126	0.210670015
6	-1.475400107	-1.685380122	2.216070160
6	-3.729470270	-0.765920055	2.581040187
1	-4.064470294	-0.007540001	3.289040238
1	-4.312270312	-0.655910047	1.663650120
1	-6.484120470	0.741760054	-1.636990119
1	-3.860020280	-1.764580128	2.991170217
1	6.483000470	0.748710054	1.638110119

1	4.064680294	-0.000860000	-3.288410238
1	-2.226240161	-4.335080314	-1.160060084
1	0.049090004	4.329460314	-1.767510128
1	2.227700161	-4.337090314	1.154140084
1	-0.050660004	4.326060313	1.771470128
6	-3.863070280	-3.729670270	-0.023710002
1	-3.837170278	-2.951600214	0.738910054
1	-4.848370351	-3.736120271	-0.491260036
1	-3.672720266	-4.683370339	0.475260034
6	3.864510280	-3.729010270	0.019060001
1	3.838310278	-2.949790214	-0.742390054
1	4.849690351	-3.735540271	0.486880035
1	3.674930266	-4.682050339	-0.481480035
6	1.655020120	3.774670273	-2.965210215
1	2.660930193	3.738520271	-2.546600184
1	1.591150115	3.031290220	-3.765950273
1	1.466070106	4.762290345	-3.396300246
6	-1.656410120	3.769890273	2.968660215
1	-1.468240106	4.757620345	3.399830246
1	-2.662310193	3.733010270	2.550080185
1	-1.591940115	3.026470219	3.769340273

Table S5. Crystal data and structure refinement for **PPD**.

Empirical formula	C56 H64 N8 O8	
Formula weight	977.15	
Temperature	293(2) K	
Wavelength	0.71073 Å	
Crystal system	Tetragonal	
Space group	P 43 21 2	
Unit cell dimensions	a = 14.7104(7) Å	α= 90°.
	b = 14.7104(7) Å	β= 90°.
	c = 23.995(2) Å	γ = 90°.
Volume	5192.4(7) Å^3	
Z	4	
Density (calculated)	1.250 Mg/m^3	
Absorption coefficient	0.085 mm^{-1}	
F(000)	2080	
Crystal size	0.200 x 0.190 x 0.170 mm^3	
Theta range for data collection	2.190 to 24.998°.	
Index ranges	-14<=h<=17, -17<=k<=17, -28<=l<=28	
Reflections collected	40315	

Independent reflections	4582 [R(int) = 0.1305]
Completeness to theta = 24.998°	99.9 %
Absorption correction	Semi-empirical from equivalents
Max. and min. transmission	0.986 and 0.983
Refinement method	Full-matrix least-squares on F^2
Data / restraints / parameters	4582 / 2 / 328
Goodness-of-fit on F^2	0.878
Final R indices [I>2sigma(I)]	R1 = 0.0775, wR2 = 0.1952
R indices (all data)	R1 = 0.1959, wR2 = 0.2357
Absolute structure parameter	2(4)
Extinction coefficient	0.0054(19)
Largest diff. peak and hole	0.281 and -0.164 e.Å^{-3}

Table S6. Crystal data and structure refinement parameter for **PP-NDI**.

Empirical formula	C34 H44 N4 O4	
Formula weight	572.73	
Temperature	293(2) K	
Wavelength	0.71073 Å	
Crystal system	Triclinic	
Space group	P -1	
Unit cell dimensions	a = 4.7183(13) Å	α= 78.569(8)°.
	b = 12.508(3) Å	β= 86.876(8)°.
	c = 13.014(4) Å	γ = 82.105(8)°.
Volume	745.4(3) Å^3	
Z	1	
Density (calculated)	1.276 Mg/m^3	
Absorption coefficient	0.084 mm^{-1}	
F(000)	308	
Crystal size	0.200 x 0.190 x 0.170 mm^3	
Theta range for data collection	2.528 to 24.998°.	
Index ranges	-5<=h<=5, -14<=k<=14, -15<=l<=15	
Reflections collected	19100	
Independent reflections	2634 [R(int) = 0.1508]	
Completeness to theta = 24.998°	99.9 %	
Absorption correction	Semi-empirical from equivalents	
Max. and min. transmission	0.986 and 0.983	

Refinement method	Full-matrix least-squares on F^2
Data / restraints / parameters	2634 / 0 / 199
Goodness-of-fit on F^2	0.892
Final R indices [I>2sigma(I)]	R1 = 0.0879, wR2 = 0.2131
R indices (all data)	R1 = 0.1903, wR2 = 0.2603
Extinction coefficient	0.089(19)
Largest diff. peak and hole	0.316 and -0.249 e.$Å^{-3}$

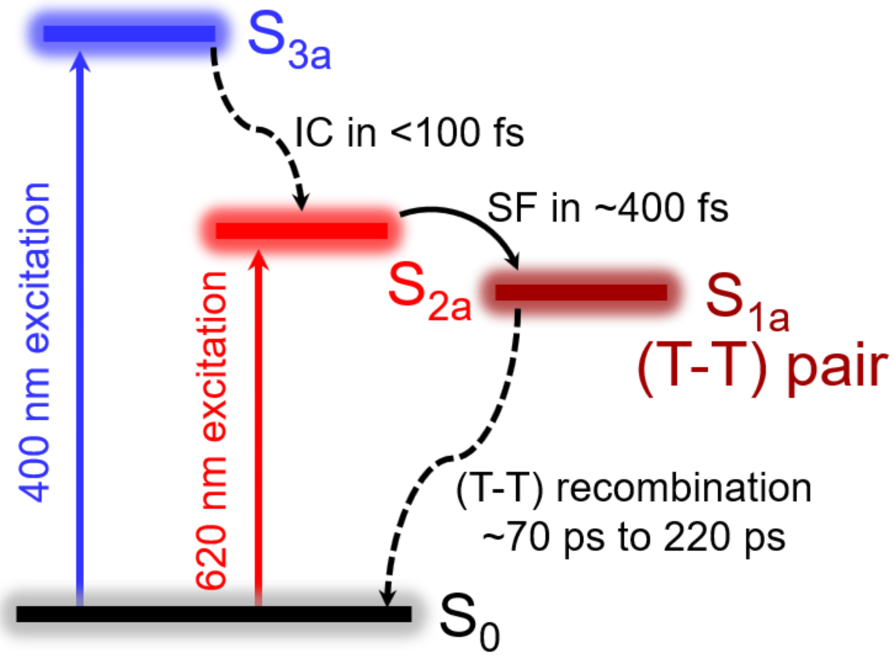

Figure S21. Energy level diagram for the SF dynamics in PPD for both 400 nm and 620 nm pump excitation. The lowest singlet state (S_{1a}) has multi-excitonic character which is an optically dark singlet state. i.e. the T-T pair state. The ICT transition leads to generation of the first optically allowed state which is designated as S_{2a}. The blue-excitation at 400 nm denotes the π-π* transition, which leads to the formation of the S_{3a} state.

References

1. Ajayakumar, M.; Asthana, D.; Mukhopadhyay, P., Core-modified naphthalenediimides generate persistent radical anion and cation: New panchromatic NIR probes. *Org. Lett.* **2012,** *14*, 4822-4825.

2. Frisch, M. J.; Trucks, G. W.; Schlegel, H. B.; Scuseria, G. E.; Robb, M. A.; Cheeseman, J. R.; Scalmani, G.; Barone, V.; Petersson, G. A.; Nakatsuji, H.; Li, X.; Caricato, M.; Marenich, A. V.; Bloino, J.; Janesko, B. G.; Gomperts, R.; Mennucci, B.; Hratchian, H. P.; Ortiz, J. V.; Izmaylov, A. F.; Sonnenberg, J. L.; Williams-Young, D.; Ding, F.; Lipparini, F.; Egidi, F.; Goings, J.; Peng, B.; Petrone, A.; Henderson, T.; Ranasinghe, D.; Zakrzewski, V. G.; Gao, J.; Rega, N.; Zheng, G.; Liang, W.; Hada, M.; Ehara, M.; Toyota, K.; Fukuda, R.; Hasegawa, J.; Ishida, M.; Nakajima, T.; Honda, Y.; Kitao, O.; Nakai, H.; Vreven, T.; Throssell, K.; Montgomery, J. A., Jr.; Peralta, J. E.; Ogliaro, F.; Bearpark, M. J.; Heyd, J. J.; Brothers, E. N.; Kudin, K. N.; Staroverov, V. N.; Keith, T. A.; Kobayashi, R.; Normand, J.; Raghavachari, K.; Rendell, A. P.; Burant, J. C.; Iyengar, S. S.; Tomasi, J.; Cossi, M.; Millam, J. M.; Klene, M.; Adamo, C.; Cammi, R.; Ochterski, J. W.; Martin, R. L.; Morokuma, K.; Farkas, O.; Foresman, J. B.; Fox, D. J. Gaussian 16, Revision C.01, Gaussian, Inc., Wallingford CT, 2016.

3. Roos, B. O., The complete active space self-consistent field method and its applications in electronic structure calculations. *Advances in Chemical Physics: Ab Initio Methods in Quantum Chemistry Part 2* **1987,** *69*, 399-445.

4. Granovsky, A. A., Extended multi-configuration quasi-degenerate perturbation theory: The new approach to multi-state multi-reference perturbation theory. *The Journal of chemical physics* **2011,** *134* (21), 214113.

5. Parker, S. M.; Seideman, T.; Ratner, M. A.; Shiozaki, T., Model Hamiltonian analysis of singlet fission from first principles. *The Journal of Physical Chemistry C* **2014,** *118* (24), 12700-12705.

6. Dunning, T. H.; Hay, P. J., Methods of electronic structure theory. *Modern theoretical chemistry* **1977,** *3*, 1-28.

7. Witek, H. A.; Choe, Y. K.; Finley, J. P.; Hirao, K., Intruder state avoidance multireference Møller–Plesset perturbation theory. *Journal of computational chemistry* **2002,** *23* (10), 957-965.

8. Granovsky, A. A., Firefly Version 8. *http://classic.chem.msu.su/gran/firefly/index.html* **2014**.

9. Neese, F.; Wennmohs, F.; Becker, U.; Riplinger, C., The ORCA quantum chemistry program package. *The Journal of chemical physics* **2020,** *152* (22), 224108.

10. Schapiro, I.; Sivalingam, K.; Neese, F., Assessment of n-electron valence state perturbation theory for vertical excitation energies. *Journal of Chemical Theory and Computation* **2013,** *9* (8), 3567-3580.